fire

MDPI

Article

Geovisualization and Analysis of Landscape-Level Wildfire Behavior Using Repeat Pass Airborne Thermal Infrared Imagery

Keaton Shennan [1,*], Douglas A. Stow [1], Atsushi Nara [1], Gavin M. Schag [1] and Philip Riggan [2]

[1] Department of Geography, San Diego State University, San Diego, CA 92182, USA; stow@sdsu.edu (D.A.S.); anara@sdsu.edu (A.N.); gschag@sdsu.edu (G.M.S.)
[2] USDA Forest Service, Pacific Southwest Research Station, Riverside, CA 96002, USA; philip.riggan@usda.com
* Correspondence: shennan.keaton@gmail.com

Abstract: Geovisualization tools can supplement the statistical analyses of landscape-level wildfire behavior by enabling the discovery of nuanced information regarding the relationships between fire spread, topography, fuels, and weather. The objectives of this study were to develop and evaluate the effectiveness of geovisualization tools for analyzing wildfire behavior and specifically to apply those tools to study portions of the Thomas and Detwiler wildfire events that occurred in California in 2017. Fire features such as active fire fronts and rate of spread (ROS) vectors derived from repetitive airborne thermal infrared (ATIR) imagery sequences were incorporated into geovisualization tools hosted in a web geographic information systems application. This geovisualization application included ATIR imagery, fire features derived from ATIR imagery (rate of spread vectors and fire front delineations), growth form maps derived from NAIP imagery, and enhanced topographic rasters for visualizing changes in local topography. These tools aided in visualizing and analyzing landscape-level wildfire behavior for study portions of the Thomas and Detwiler fires. The primary components or processes of fire behavior analyzed in this study were ROS, spotting, fire spread impedance, and fire spread over multidirectional slopes. Professionals and researchers specializing in wildfire-related topics provided feedback on the effectiveness and utility of the geovisualization tools. The geovisualization tools were generally effective for visualizing and analyzing (1) fire spread over multidirectional slopes; (2) differences in spread magnitudes within and between sequences over time; and (3) the relative contributions of fuels, slope, and weather at any given point within the sequences. Survey respondents found the tools to be moderately effective, with an average effectiveness score of 6.6 (n = 5) for the visualization tools on a scale of 1 (ineffective) to 10 (effective) for postfire spread analysis and visualizing fire spread over multidirectional slopes. The results of the descriptive analysis indicate that medium- and fine-scale topographic features, roads, and riparian fuels coincided with cases of fire spread impedance and exerted control over fire behavior. Major topographic features such as ridges and valleys slowed, or halted, fire spread consistently between study areas. The relationships between spotting, fuels, and topography were inconclusive.

Keywords: wildland fire; geovisualization; thermal imagery; fire rate of spread; extreme wildfire event

check for updates

Citation: Shennan, K.; Stow, D.A.; Nara, A.; Schag, G.M.; Riggan, P. Geovisualization and Analysis of Landscape-Level Wildfire Behavior Using Repeat Pass Airborne Thermal Infrared Imagery. *Fire* **2023**, *6*, 240. https://doi.org/10.3390/fire6060240

Academic Editors: Aqil Tariq and Na Zhao

Received: 8 May 2023
Revised: 14 June 2023
Accepted: 14 June 2023
Published: 16 June 2023

Copyright: © 2023 by the authors. Licensee MDPI, Basel, Switzerland. This article is an open access article distributed under the terms and conditions of the Creative Commons Attribution (CC BY) license (https://creativecommons.org/licenses/by/4.0/).

1. Introduction

Increasingly, wildland fires (wildfires) threaten, heavily disturb, or destroy human and ecological communities and may leave lasting ecological and environmental impacts on burned areas. With extensive residential development within and extending wildland urban interfaces (WUI), wildfires pose a growing threat to people and property throughout the world [1]. Between 1990 and 2010, the WUI was the fastest growing land use type in the conterminous United States in terms of land area and number of new houses [2]. Given the projected increase in wildfire occurrence within the conterminous United States [3], understanding wildfire behavior is more important than ever.

Wildfires are a common occurrence in the Southern California region, and understanding wildfire behavior in this region will help with wildfire preparedness and suppression efforts, as well as wildfire behavior modeling. Fuel, weather, and topography are the three main components of the wildfire environment that influence behavior. Chaparral and related shrublands are notable vegetation communities to consider because they are the predominant land cover for much of where fires occur in Southern California [4] (p. 118).

The 2019 WUI Fire Operational Requirements and Capability Analysis Report of Findings [5] evaluates the potential of new and existing technologies to impact multiple aspects of wildland fire fighting. Pre-incident modeling, fire modeling validation, and fire modeling accuracy are three of the main knowledge gaps highlighted in the report [5]. Wildfire modeling platforms such as Fire Area Simulator Model (FARSITE) [6], Wildfire Analyst [7], Fire Logic Animation (FLogA) [8], and WIFIRE [9] are capable of predictive wildfire modeling, with some being able to provide real-time, data-driven simulations. However, direct observations, measurements, or estimates of wildfire behavior properties at landscape scales for use in designing and validating fire models are challenging to make due to safety and logistics limitations. While these applications provide valuable information regarding fire behavior and its control by fuel, weather, and topographic factors, there have been few developments in visualizing more site-specific aspects of wildfire behavior. Understanding wildfire behavior at landscape scales helps fill gaps in information and knowledge by providing finer scale information regarding wildfire interactions with environmental variables.

The primary fire processes and behavior properties examined in this study were rate of spread (ROS), spotting, fire spread impedance, and spread over multidirectional slopes. Wildfire models incorporate or simulate many of these wildfire behavior components, with some also providing real time simulations [6–9]. Others focus specifically on visualizing specific drivers of fire spread, such as tree morphology [10]. While researchers achieve major advancements in wildfire modeling and three-dimensional visualization of simulation results, these depictions typically do not focus on visualizing components of wildfire behavior in attribute space. Translating science to practice and interdisciplinary work is a major challenge related to the implementation of geovisualization [11]. Visualizing attributes such as ROS, fire intensity, and elevation profiles can provide unique insight into fire behavior while also communicating the attributes with professionals and other academics more effectively. A common visualization graphic for ROS and shape and size of fires is the ellipse, depicting the length-to-width ratio that is governed by windspeed and slope steepness and from which spread distance, perimeter, and area of fire can be calculated as direct outputs [12–14]. Alternatives to the ellipse design were proposed but have not been widely adopted [14]. One objective of this paper is to propose an alternative three-dimensional (3D) visualization for ROS. However, stakeholders need to be aware of the limitations of visualizations and the underlying information and factors behind them [15].

Applications of geovisualization tools include visualizing fire features derived from airborne thermal infrared (ATIR) imagery of active portions of fire perimeters or landscape-scale sequences such as those described by Stow et al. [16,17]. Analysis of how weather, fuel, and topography interact at a landscape level for real wildfire events is needed to supplement laboratory studies that typically focus on one of these three variables exclusively [18,19]. There is a need for better understanding wildfire events at finer spatial and temporal scales than are achievable with satellite thermal infrared sensing, which can be achieved with time sequential ATIR imaging. The remote sensing of wildfires using satellite imagery provides useful information regarding burn, including detection and mapping [20,21], but airborne infrared radiometers offer greater flexibility than satellite systems for the remote sensing of wildfires. Airborne infrared radiometers can provide detailed, frequent, high-resolution data regarding the components of fires, such as fire-line ROS and acceleration and spotting [22]. However, high radiances associated with wildfires can pose challenges for infrared fire imaging, and many infrared imagers and infrared spectrometers are incapable of measuring infrared light from large wildfires [22], leading to the development of specific systems to overcome these challenges, such as the FireMapper and FireMapper 2.0 systems [23,24]. Repeat pass ATIR imagery and imagery from unmanned aerial systems can both be used to estimate ROS from fires [16,17,25]. The geovisualization tools developed in this study are aimed at providing tools for understanding nuanced information regarding interactions between fuels, weather, and topography using fire features derived from ATIR imagery sequences.

The objective of this paper is to determine the utility of geovisualization tools for the descriptive analysis of landscape-level wildfire behavior. Filling the knowledge gaps mentioned above is the motivation for addressing the following research questions:

1. What is the utility of dynamic visualizations and descriptive analyses of wildfire behavior based on spatial-temporal patterns and features of brightness temperature derived from ATIR time sequential imagery?
2. What aspects of fire behavior can be better understood using fire features derived from ATIR imagery captured in short-interval sequences?

2. Methods

2.1. Wildfire Study Area and ATIR Imagery

To address the research questions, this work focuses on developing, testing, evaluating, and implementing tools to conduct descriptive analyses of fire spread behavior, using the Thomas and Detwiler fires, which burned in the Southern California region in 2017, as case studies (Figure 1).

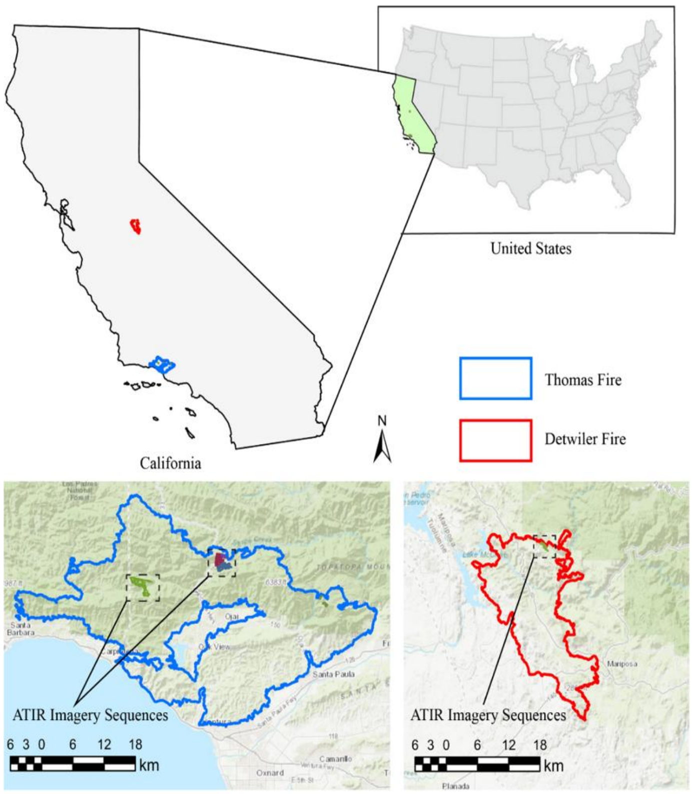

Figure 1. Study area: burn extents for the Thomas (in blue) and Detwiler (in red) Fires in California, USA [26]. The Detwiler Fire ignited 7 July 2017 in Mariposa County, California, and was not fully extinguished until 9 January 2018. The fire burned over 32,860 ha and was active for 176 days. The sequence was captured using repeat pass ATIR imagery on 20 July 2017, between 1:47 PM and 9:22 PM PST; the active front was captured moving downhill through herbaceous vegetation into an area with denser medium and large shrub coverage.

The Thomas Fire began on 4 December 2017, in Ventura County. By the time it was fully contained on 12 January 2018, the Thomas Fire had burned into Santa Barbara County and burned more than 113,715 ha [27]. Low fuel moisture content of abundant fine fuels from a wet 2016–17 winter [27] and Santa Ana wind conditions played a significant role on the behavior and severity of the Thomas Fire [27,28]. The primary types of vegetation consumed were chaparral and coastal sage scrub.

The ATIR image data set used in this study consists of geoprocessed FireMapper 2.0 image sequences: four ATIR repetitive imagery sequences for the Thomas Fire, and one for the Detwiler Fire (Figures 1 and 2). The timing and other specifics of the ATIR imaging sequences are listed in Table 1. Only small portions of the overall burn area were captured by the time sequential ATIR image frames. However, the finer spatial and temporal scale of this imagery is useful for understanding landscape-level fire behavior.

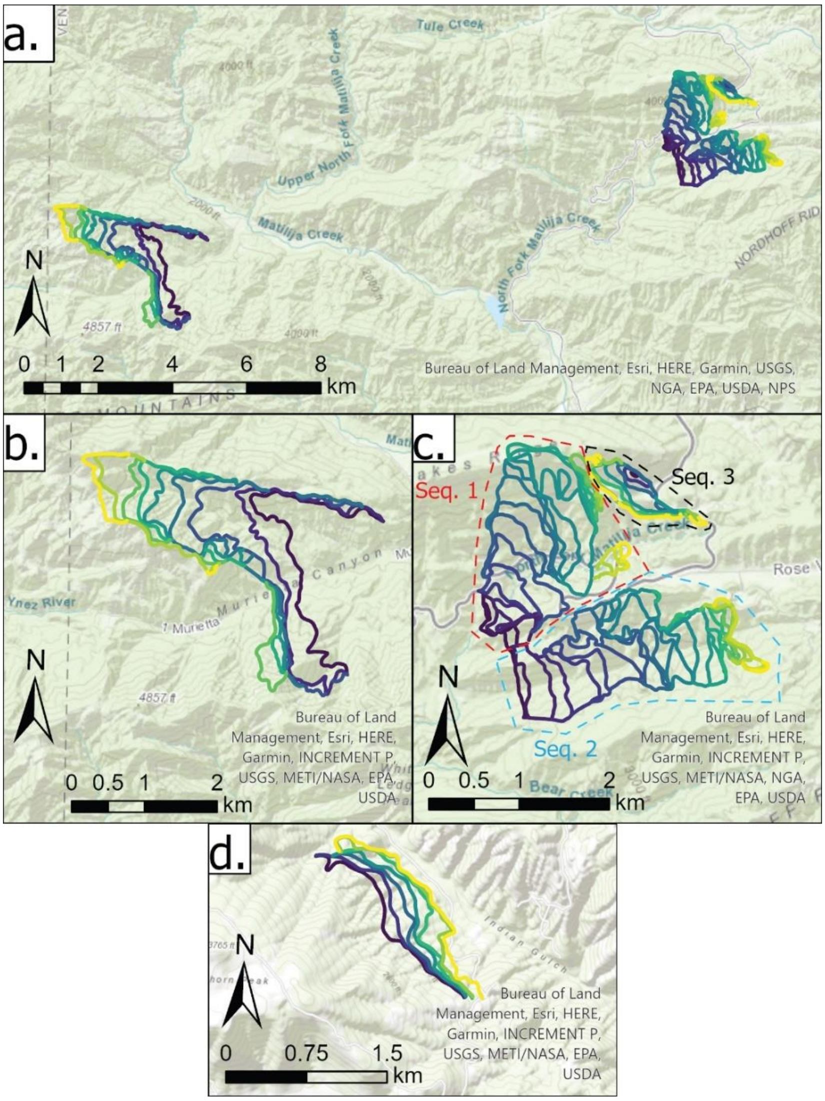

Figure 2. Active fire fronts derived from ATIR imagery sequences—all Thomas Fire sequences (**a**), Thomas Sequence 4 (**b**), Thomas Sequences 1–3 (**c**), Detwiler Fire (**d**). Progression of color spectrum displays the advancement of fire fronts within each sequence from beginning (purple) to end (yellow) [26,29].

Table 1. Airborne thermal infrared imagery metadata from Schag et al. [30].

Sequence	Date (mm/dd/yyyy)	Time Extent (PST)	Passes	Frames Per Pass	Average Time between Successive Passes (min)	GSD (m)
Thomas 1	12/08/2017	2:23:12 to 5:36:11 PM	23	30–90	10:09	10
Thomas 2	12/08/2017	2:22:54 to 5:46:11 PM	26	30–90	8:24	10
Thomas 3	12/08/2017	4:29:49 to 5:12:19 PM	7	15–30	7:05	10
Thomas 4	12/09/2017	4:33:44 to 5:22:48 PM	9	30–35	6:08	10
Detwiler	07/20/2017	3:24:57 to 4:13:30 PM	7	25	8:07	13

We visualized data derived from these two wildfire events in a three-dimensional (3D) environment to further explore environmental controls on fire spread. Three-dimensional visualizations were created using a 10 m spatial resolution digital elevation model (DEM) from the National Elevation Dataset from the United States Geological Survey (USGS) as the elevation source [31]. Existing maps of vegetation growth forms (mainly herbaceous vegetation, shrubs and trees, dead trees, and barren rock and soil) were derived from color infrared orthoimagery with 0.6 m ground sampling distance (GSD) produced by the United States National Agriculture Imagery Program (NAIP) using Google Earth Engine [32,33]. Active fire front locations and ROS vectors were derived from the ATIR imagery using the methods described by Stow et al. [16,17] and Schag et al. [30]. Using the active fire front curves delineated from ATIR imagery, spread vectors were generated by automatically placing evenly spaced points 30 m apart along the time = n (start) front curve, which were then used to generate local normal polyline connections to time $n + 1$ curves. ROS was calculated using the geodesic straight-line distance travelled along the spread vector divided by the time interval between successive fire front locations [16,17,30]. The 3D web scene facilitated the visualization of active front locations and ROS vectors for analyzing the relationships between fuels, topography, and other environmental controls on fire spread.

2.2. Dynamic Visualizations of Wildfire Processes

Interactive 3D visualizations of wildfire dynamics allow users to interact with and analyze the data in a way that may be more effective than more traditional two-dimensional methods. To facilitate the geovisualization and visual analysis of wildfire behavior, we developed a web application containing custom 3D tools for visualizing fire spread [34,35]. The web application contained NAIP imagery [32] of the study area, growth form maps, TIR imagery sequences, fire front delineations, and ROS vectors for the Thomas and Detwiler fire sequences (Figure A1).

To better understand the patterns of fire spread, we designed and evaluated 3D spherical graphics termed the Rate of Spread Sphere (ROSS), as depicted in Figure 3 (Figure A2). The directional bearing of a spread vector is located along the circumference, with bearing labels at 90-degree intervals, as seen in Figure 3a. The x-axis of the sphere represents the magnitude of the ROS in m min^{-1}; the yellow rings radiating from the center of the sphere in Figure 3a represent increasing 20% increments of ROS. As seen in Figure 3b, the y-axis of the sphere incorporates the average slope angle in degrees for each ROS vector. The ROS vectors are depicted as green (positive slope angle) and blue (negative slope angle) lines that originate in the center of the sphere and radiate out according to their bearing, ROS, and average slope angle (Figure 3d). When available, the wind bearing for the nearest hourly wind data from RAWS stations and the FireBuster model [36] are displayed by orange and gold vectors, respectively (Figure 3a,c,d). Upon selection, these vectors display information regarding average wind speed (m/s), bearing, and time of measurement. This visualization tool supports the analysis of ROS trends in 3D attribute space, providing insights on the patterns and relationships of ROS magnitude and directionality with terrain slopes. Data inputs for this visualization tool are ROS vectors that include information regarding bearing and spread rate, terrain slope, and wind vectors generated from RAWS data or FireBuster [36] estimates with attributes for time of measurement, bearing, and average windspeed (m/s).

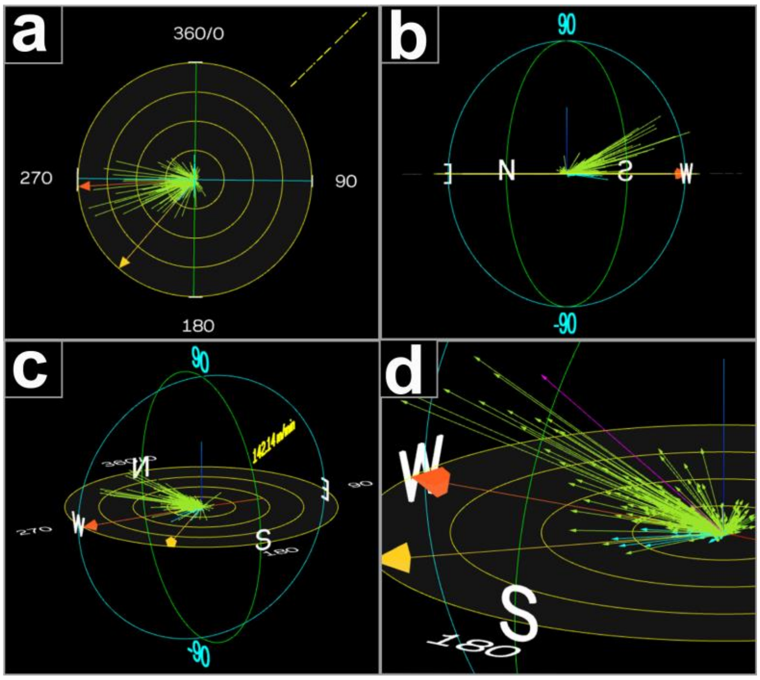

Figure 3. Four views of 3D ROS Sphere (ROSS) visualization—x-axis (**a**), y-axis (**b**), perspective view (**c**), detail view displaying ROS vectors with positive slope angle in green and negative slope angle in cyan (**d**).

To visualize fire spread over multidirectional slopes (i.e., when fire spread vectors extend both up and down terrain slopes), we generated elevation profiles of TIR brightness values associated with positions of estimated spread vectors. Through the selection of multiple spread vectors in a 3D web map visualization, a plot of the elevation profiles was generated with the ability of "mouseover" querying. This visualization approach enables a user to dynamically interact with the graphs by highlighting the elevation at the cursor location for each of the vectors along the length of the spread vector.

To evaluate the effectiveness of these visualizations, we solicited feedback from academic and professional scientists and technologists who study and model wildfire behavior. We conducted a survey [37] on the effectiveness of the visualization platform in terms of interoperability, clarity of the visualization, and needed improvements (Appendix C).

Exploratory Analysis of Fire Behavior

An exploratory visual analysis was conducted using the aforementioned 3D modeling and geovisualization environment to learn more about what aspects of fire behavior can be better understood by studying dynamic fire features extracted from time-sequential ATIR imagery. The general research approach and flow are depicted in Figure 4. We focused on analyzing fire behavior components relating to ROS and slope of spread vectors between each front location, landforms, changes in slope along spread vectors, multiscale analysis of ROS, and spread over multidirectional slopes. Spotting occurrence and fire spread impedance were also assessed. ROS was visualized using the ROSS 3D spherical visualization tool described above (Figure 3). The 10-m DEM provided elevation information for visualizing terrain relief, and an average slope angle and elevation profile were generated for each ROS vector from this DEM. To identify and exaggerate local minimum and maximum elevation values, we generated an enhanced topographic raster to accentuate these differences. We used a focal statistics tool to calculate the average elevation change for 40 $\times$ 40 m cell regions of the original DEM. The resultant raster was subtracted from the original DEM to discern whether a raster cell was above (positive) or below (negative) the neighborhood average for the purpose of accentuating relative changes in elevation across the study area. Slope angle and slope aspect rasters were also created using the 10-m DEM.

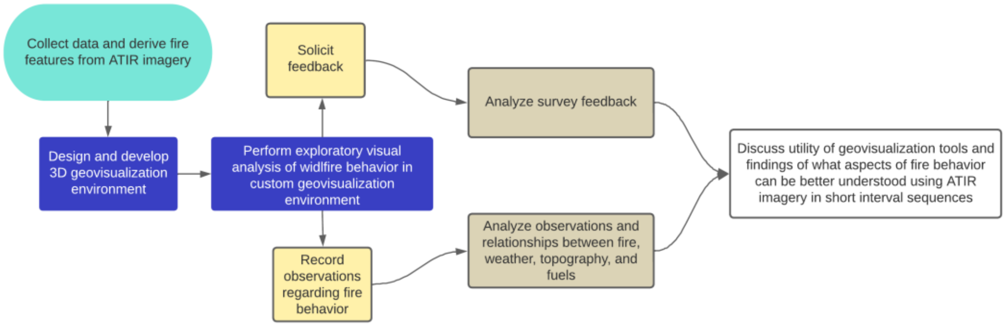

Figure 4. Flow chart diagram of research methods.

The 5th and 95th percentile of the frequency distribution of magnitudes of ROS vectors for each of the active front sequences were selected to gain a general understanding of the vegetation and terrain controls associated with the extreme (lowest and highest) estimated ROS [30]. For these selected ROS vectors, observations regarding slope, elevation, spread rate, land cover types, and context associated with the preceding and subsequent active front locations were logged and organized in a spreadsheet. To identify unique cases of landscape-level fire behavior, graphs depicting slope versus ROS were generated to help identify cases where either ROS was high and slope was low, or conversely, if ROS was low and slope was high. The ROS vectors were visually analyzed using the ROSS (Figure 3) and 3D web scene to explore patterns and apparent relationships between terrain, vegetation, and rate of spread for each sequence of fire fronts (Figure 5).

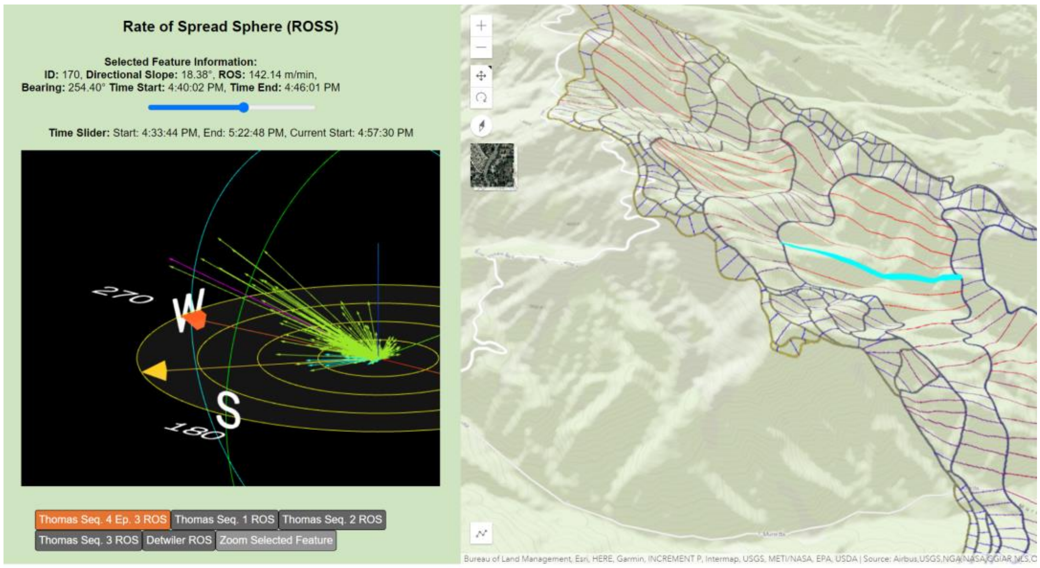

Figure 5. View of the web application displaying interaction between the selected ROSS spread vector (purple, left) and the map spread vectors (cyan, left) [26,29].

We also identified landscape features that appeared to impede fire spread. Specific features that were identified included ridges, drainage areas, riparian areas, rock outcrops, and roads. GIS layers depicting landcover were overlaid to identify where the fire spread intersected with the various fuel breaks and barriers [38]. At places where natural barriers were identified, we assessed the extent to which rock outcrops and similar natural features impeded fire spread, to better understand their control on landscape-level fire behavior.

3. Results

3.1. Dynamic Visualizations of Wildfire Processes

3.1.1. Web-Based Geovisualization Tools

A survey concerning the utility and effectiveness of the 3D geovisualization environment was emailed to 28 academic and professional scientists and technologists who study and model wildfire behavior and yielded 6 results for a response rate of 22%. The nature of feedback on the user interface from those who tested the overall utility and effectiveness of the tools appeared to depend on prior exposure to GIS. Survey respondents (n = 6) familiar with GIS tools generally found the user interface simple and informative, while others found the user interface challenging to navigate and emphasized the utility of the background information as a guide.

Survey respondents suggested these tools are useful for determining the relative importance of fuels, slope, and variations in fire growth over time and postfire spread analysis but may be of limited utility in an operational setting. Some respondents suggested the ROSS (Figure 3) was useful for visualizing differences in spread magnitudes within and between sequences over time, fire spread model validation, and the relative contributions of fuels, slope, and weather at any given point in the sequence. The mean usefulness score of the ROSS was 3.7 out of 5 (n = 6). Survey respondents found the most effective aspects of the visualization tools to be the upslope and downslope characterization of fire spread. They underscored the utility of these tools for identifying subtle influences of the landscape on ROS and visualizing fire spread over multidirectional slopes.

Improving interaction between the ROSS and the application's web map displaying fire behavior features and ATIR imagery was the predominant recommendation for the visualization tools. The average effectiveness score was 6.6 (n = 5) for the visualization tools on a scale of 1 (ineffective) to 10 (effective), with a minimum of 3 and a maximum of 9. Including satellite and ATIR imagery, sun angle, and precipitation data layers were recommended as useful for facilitating fire spread analyses. Users indicated that these tools may be useful for fire simulation and modeling validation and calibration, qualitative wildfire studies, and for focusing additional research and analysis.

3.1.2. Enhanced Topographic Raster

The enhanced topographic raster graphic portrayed local topographic features more effectively than the unenhanced DEM (Figure 6). The hillshade raster [29] provided more detail regarding fine-scale topographic variations, but less information regarding local elevation changes than the enhanced topographic raster.

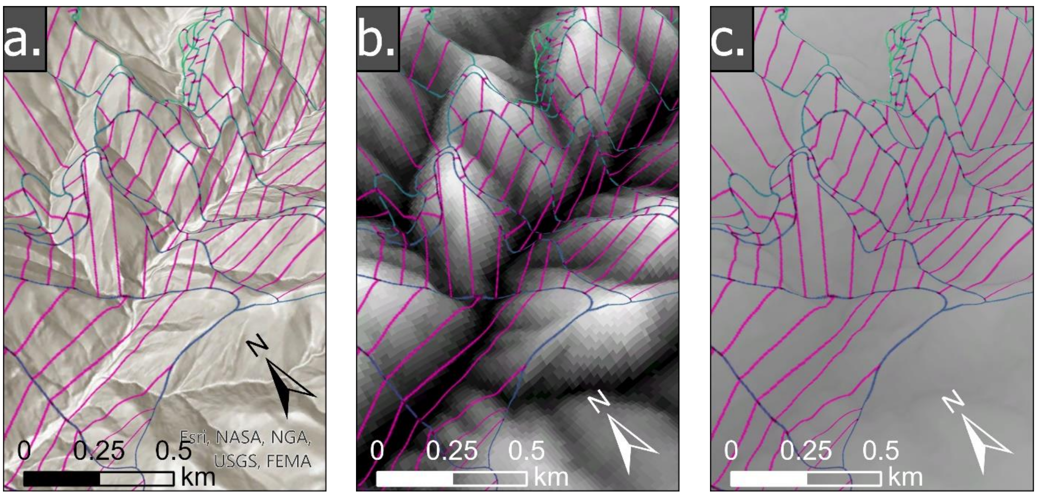

Figure 6. Raster underlays with 3D view of Thomas Fire Sequence 2: Esri hillshade [29] (**a**), enhanced topographic raster (**b**), and USGS DEM [31] (**c**), with rate of spread vectors (purple) and fire front delineations colorized from purple (earlier) to yellow (later).

3.2. Visual/Descriptive Analysis of Wildfire Spread—Fire Behavior Identified through Geovisualization of Rapid Sequence ATIR Imagery

3.2.1. Influence of Topography and Fuels

Major and minor topographic features appeared to exert control on fire spread for the study fires, as observed from geovisualization of the ATIR sequences. Prominent ridgelines and valleys were associated with areas of fire spread impedance, and sometimes acted as fire boundaries [28,39]. At fine scales, fuel type and slope steepness were dominant influences on fire spread [40]. In some instances, local spurs and draws appeared to coincide with local acceleration and deceleration of the fire spread, respectively. However, some occurrences of high ROS coincided with high variation in local topography during Thomas Fire Sequence 4.

Ridgelines appeared to contribute to fire spread impedance during Thomas Fire Sequences 1, 2, and 4. ROS vectors in these areas generally exhibited low ROS (within the 5th percentile of the frequency distribution of magnitudes of ROS) (Table 2). The average directional slope among the spread vectors in the 5th percentile of the frequency distribution of magnitudes of ROS was negative in all cases, except for Thomas Fire Sequence 4 (Table 2).

Table 2. General and 5th and 95th percentile of frequency distribution of magnitudes of slope and rate of spread for Thomas Fire sequences (from Schag et al. [30]).

Sequence	Slope Trend (deg)	ROS Trend (m min^{-1})	5th Percentile Mean Slope (deg)	5th Percentile Mean ROS (m min^{-1})	95th Percentile Mean Slope (deg)	95th Percentile Mean ROS (m min^{-1})
Thomas Fire Sequence 1	19.54	9.76	−12.02 (n = 18)	1.37 (n = 18)	25.77 (n = 18)	45.45 (n = 18)
Thomas Fire Sequence 2	10.53	11.74	−1.78 (n = 21)	1.09 (n = 21)	6.34 (n = 21)	41.58 (n = 21)
Thomas Fire Sequence 3	13.50	11.86	−18.60 (n = 7)	0.90 (n = 7)	18.76 (n = 7)	26.25 (n = 7)
Thomas Fire Sequence 4	11.06	48.48	4.77 (n = 23)	2.06 (n = 23)	19.99 (n = 23)	91.94 (n = 23)
Detwiler Fire	−10.01	6.30	−9.33 (n = 9)	0.51 (n = 9)	−2.48 (n = 9)	21.32 (n = 9)

Cases of slow upslope spread were typically limited to fire spread along the edges of roads, or at the peripherals of the active front where the fire spread hovers near a major ridgeline. An observation of fire spread slowing along the backside of a ridge occurred as the fire spread passed the crest of the ridge and began moving downslope on the back side of the ridge during Thomas Fire Sequence 1. ROS slowed dramatically for this sequence during this interval compared to fire spread rates estimated for the preceding imaging passes 15 min before.

Rapid ROS coincided with smooth, steep terrain covered in shrub-dominant fuels for Thomas Fire Sequence 1. Preheating of fuels on steep slopes often contributes to increased fire spread rates [18], yet the fastest ROS during Thomas Fire Sequences 2 and 4 traversed multiple slope facets while moving parallel with the valley floor. The highest (fastest) magnitudes of the frequency distribution of magnitudes of ROS primarily corresponded to upslope spread at a steeper angle than the overall trend, except for the Detwiler Fire Sequence (which was almost entirely captured during downslope fire spread) and Thomas Fire Sequence 2. Generally, the areas with the highest ROS followed the general directional trend of the fire, moved upslope, and occurred in areas of homogeneous vegetation. Other studies on topographic controls also found that fire generally spreads more rapidly up steep slopes due to convective upslope heating [41].

Past studies report that valley bottoms exert control over fire boundaries [39,41]. During Thomas Fire Sequences 2 and 4, spread along the valley floor moved slower than spread moving horizontally across the adjacent slopes. Spread along the valley floors encountered denser fuel types associated with riparian areas, whereas spread along the hillsides primarily encountered shrub and herb fuel types. Despite local deceleration in riparian areas, the ROS observed is still much higher than the overall trend for either sequence.

Fire spread behavior over fine-scale topographic features varied between sequences. During Thomas Fire Sequences 1 and 2, minor topographic features appear to have exerted greater control over fire spread, whereas they appeared to exert less control for Thomas Fire Sequence 4. However, during Thomas Fire Sequence 4, the highest and lowest ROS recorded during the sequence occurred over a short, approximately 15-min, window, illustrating the space-time variability of ROS influenced by localized controlling variables.

For the duration of Thomas Fire 1 and 2 imaging sequences, an area between the two advancing lobes remained unburned. The advancing joined lobes of Thomas Fire Sequences 1 and 2 remained joined before diverging into two local valleys on either side of a major ridge. Minor topographic features appear to have influenced fire spread at the point of divergence as the fire front delineations align with and move parallel to two minor spurs' ridgetops (Figure 7) and slows as the fire spreads downslope within the draw. Within 150 m of the perimeters surrounding the unburned area, ROS among spread vectors for Thomas Fire Sequences 1 and 2 were similar to the overall sequence trend but varied at finer spatial scales. The two lobes surrounding the unburnt area traversed shallower (near horizontal) slopes compared to the overall trends. Fuels surrounding this area consisted of shrubs with interspersed patches of herbaceous vegetation.

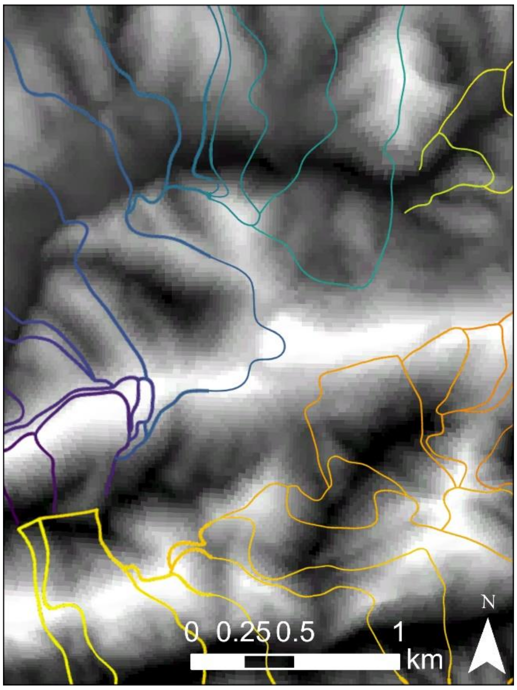

Figure 7. Unburned area (center region) between Thomas Fire Sequences 1 (top 2/3, viridis color palate (purple—earlier, yellow—later), spreading NNE–NE) and 2 (bottom 1/3, yellow (earlier) to red (later), spreading ENE–E) with topographic focal raster underlay.

Fire spread during Thomas Fire Sequence 4 generally trended upslope as it traversed multiple interlocking spurs while it burned through the valley (Figure 8). As Thomas fire Sequence 4 progressed, large lobes appeared on both hillsides adjacent to the valley and appeared to spread faster than the fire spread along the valley floor. The SW–SSW fire spread on the southern slope moved diagonally upslope, whereas the fire spread in a westerly direction on the northern slope generally moved horizontally across the slope. A combination of thicker riparian fuels and higher local variation in topography appeared to contribute to controls on fire spread in the valley floor.

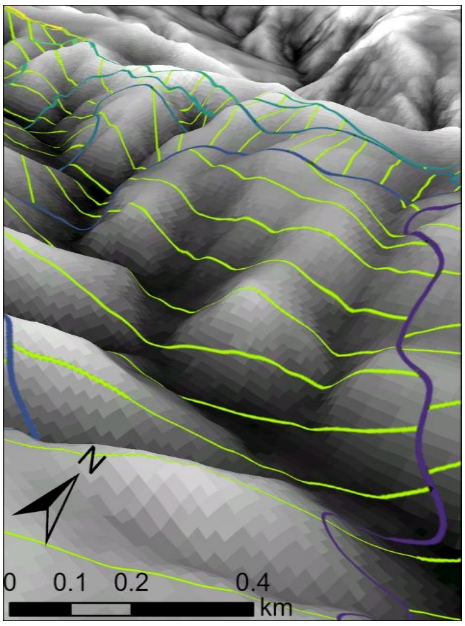

Figure 8. Westerly fire spread (ROS vectors in green, fire front delineations start as purple and move towards yellow as the sequences progresses) over multidirectional slopes during Thomas Fire Sequence 4.

Areas of homogeneous fuels typically corresponded to areas with faster ROS, and vice versa for areas with heterogeneous fuels. Vegetation growth form and bare cover associated with the 5th percentile (i.e., slowest) ROS vectors tended to vary and be heterogeneous, whereas the 95th percentile (i.e., fastest) ROS vectors typically moved through homogeneous shrub dominated terrain [42,43]. For all study sequences but Thomas Fire Sequence 2, the predominant fuel type was a chaparral shrub dominant mix with patchy herbaceous vegetation and areas of barren soil and rock. An association between slow ROS and areas with heterogeneous vegetation, rock bands, and other barren zones or roads is readily apparent.

To summarize, the slowest ROS occurred for areas of heterogeneous fuels, fire spread that moved over multiple slope facets in a short distance, and at ridgelines. This is consistent with other studies that found diverse landcover, fuel discontinuity, and topographic roughness limit fire size and fire spread [42]. Generally, the areas with the highest ROS followed the general directional trend of the fire, moved upslope, and occurred in areas of homogeneous vegetation. Other studies on topographic controls also found that fire generally spreads more rapidly up steep slopes due to convective upslope heating [41].

3.2.2. Cases of Fire Spread Impedance

Cases of fire spread impedance identified through the geovisualization of wildfire features coincided with roads, ridgelines, heterogeneous vegetation, riparian areas, and topographically diverse areas. During Thomas Fire Sequence 1, prominent bands of rock outcrops 70–90 m wide (in direction of fire spread) impeded fire spread between two lobes advancing uphill (Figure 9). After encountering the rock outcrop, the local ROS accelerated as the fire moved up a 20–25-degree slope (Figure 9). The most rapid spread for Thomas Fire Sequence 1 occurred on either side of the rock band during the following interval of the sequence and coincided with 20–25-degree upslope movement and homogeneous fuels consisting primarily of shrubs. Spotting is clearly evident in the TIR imagery in advance of the active fire front prior to the lobes expanding upslope; however, no spot fires can be seen in the area where the lobes developed in the preceding TIR image. Another occasion of a fast-spreading lobe appeared during Thomas Fire Sequence 2, where a fast-spreading lobe on the northern flank travelled upslope and perpendicular to the general direction of the fire (Figure 10).

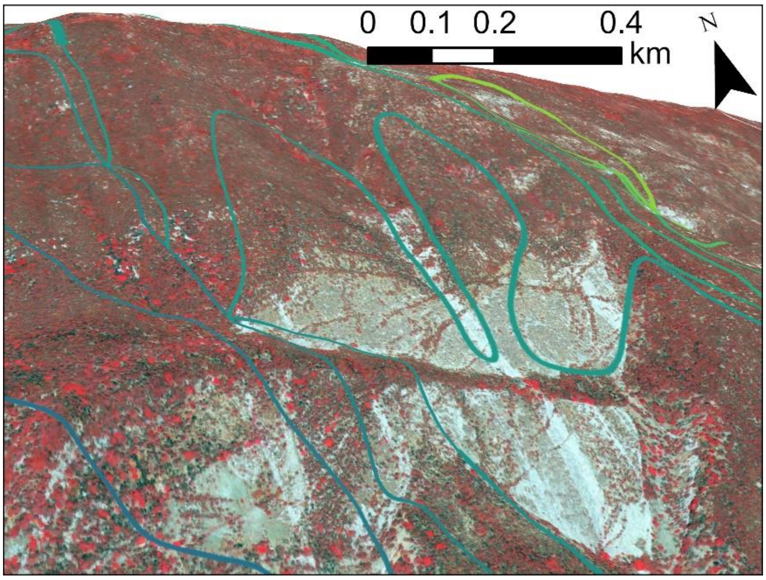

Figure 9. Perspective view of Thomas Sequence 1 fire spread upslope with NAIP imagery [32] (acquired July 2016) underlay displayed as false color composite (NIR, R, G band combination). Fire front delineations start as purple and move towards yellow.

Figure 10. Lobe appearing during the final intervals of the Thomas Fire Sequence 2 in blue (earlier) to yellow (later) with NAIP imagery [32] (acquired July 2016) underlay displayed as false color composite (NIR, R, G band combination).

During the final passes of Thomas Fire Sequence 2, a lobe developed and moved diagonally SE relative to the general direction of the fire spread (Figure 10). The bearing of the local fire spread in the lobe moved from ENE to SSE as it began to decelerate. Areas of decelerating fire spread corresponded to local areas of downslope fire spread. The active front west of the lobe remained separated from the lobe itself for the duration of the sequence. Areas of thick riparian fuels between the two active fronts aligned with the perimeter of the fire spread for the final passes of the sequence.

Roads were the most effective barrier to fire spread when the spread was moving parallel to the road. Large ridges and valleys also consistently controlled fire spread. Narayanaraj et al. [44] concluded that when roads were present and their effects significant, they were the strongest environmental constraint on boundary locations. A similar impedance at fire boundaries was observed in the Thomas Fire 1, 2, and 3 sequences as the fire encountered California State Route 33 (SR33, also referred to as the Maricopa Highway) (Figure 11). The ability of the road to impede fire spread varied between sequences.

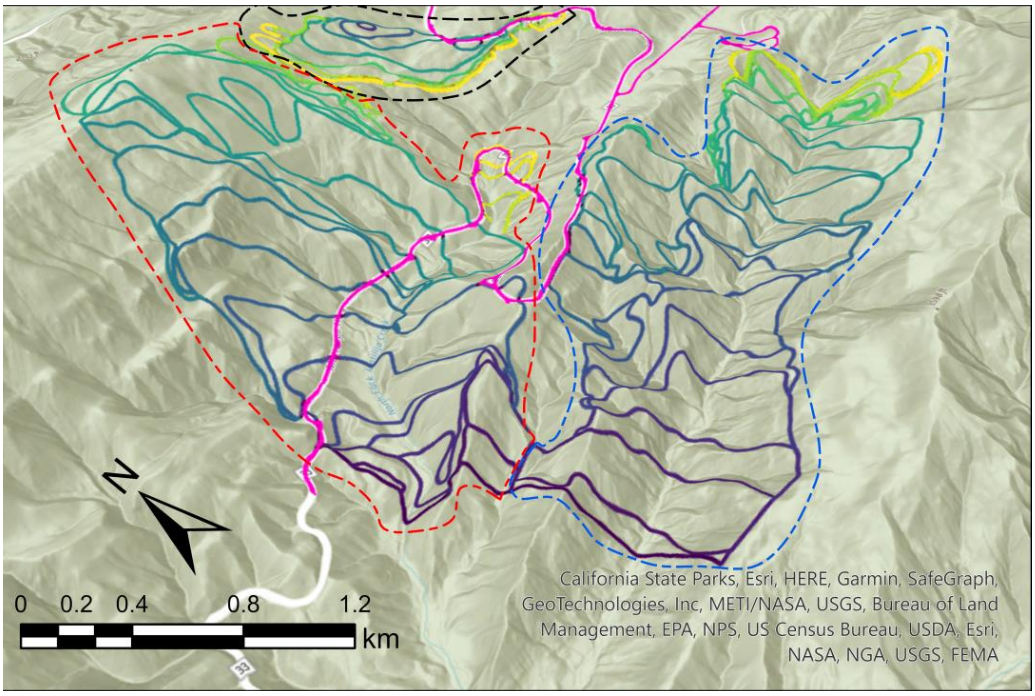

Figure 11. Three-dimensional view of active fire front positions for Thomas Fire Sequences 1 (red), 2 (blue), and 3 (black). Earlier passes start as purple and move towards yellow as the sequences progress. Portions of California State Route 33 (SR33, also referred to as the Maricopa Highway) near the sequences are displayed in magenta [26,29].

During Thomas Fire Sequence 1, the fire was moving roughly 50–70 degrees clockwise from the road. Where SR33 corresponded to local boundaries of the active front during the latest passes of Thomas Fire Sequence 1, the fire spread moved parallel to the road. Where SR33 effectively aided fire spread impedance, the local ROS for spread vectors was similar to the spread that crossed SR33, averaging 12.45 m min^{-1} (n = 14). The directional slope was much shallower, averaging 2.19 degrees (n = 14). Fuel types for both aforementioned areas consisted of thicker riparian vegetation (including trees) and shrubs. For Thomas Fire Sequence 2, cases of fire spread impedance along SR33 were clearest as it crossed from the south to the north side of the ridge. For Thomas Fire Sequence 3, the road acted as an effective control on fire spread for the duration of the sequence, with no instances of the fire crossing the road at the time of imaging. Additional suppression efforts along SR33 were possibly in place given the special circumstances surrounding the Thomas Fire Sequence 3 ignition. SR33 may have acted as a fortified fire barrier given that Thomas Fire Sequence 3 was a backfire ignited by the California Department of Forestry and Fire Protection (CAL FIRE). The fire primarily spread downslope towards the approaching active front of Thomas Fire Sequence 1.

3.2.3. Spotting

Spotting is evident as small hotspots in advance of the active front during Thomas Fire Sequences 1 and 4. Fire spots occurred approximately 160 m in advance of the active front during the last interval (5:46:11 PM) of Thomas Fire Sequence 1 (Figure 12a). The nearest hourly average wind speed estimates from the Rose Valley RAWS station (0.4 m s^{-1}, 5–6 km east) and FireBuster model (1.8 m s^{-1}) do not indicate higher windspeeds during times of greater spotting activity. Smaller burning patches are detectable behind the active front during this time. This portion of the fire spread upslope through riparian fuels into an area with steeper slopes and primarily shrub fuels. During Thomas Fire Sequence 4, spotting was also evident in advance of the active front between 4:52:47 PM and 4:57:30 PM (Figure 12b). As in Sequence 1, the nearest hourly windspeed estimates from the Casitas RAWS station (2.7 m s^{-1}, 11.5 km south) and FireBuster [36] model (6.71 m s^{-1}) do not indicate that higher windspeeds occurred during times of greater spotting activity. The burn area of the spot fires remained stable for approximately 20 min and then increased. These instances of spotting occurred upslope of the active fire fronts in the direction of spread, while the fire spread appeared to accelerate in the preceding intervals. Fuels in this area primarily consisted of homogeneous shrub fuels. No association between areas of spotting and specific types of vegetation is apparent when comparing TIR-derived brightness temperature and NAIP-derived growth form data.

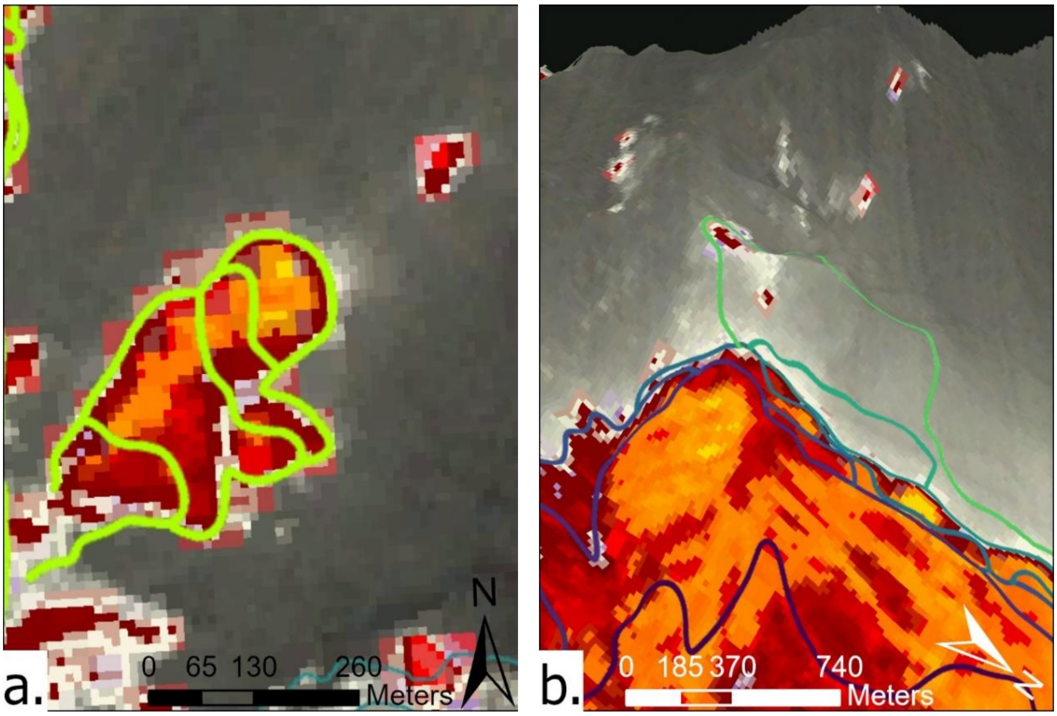

Figure 12. Spotting in advance of the active fire front during Thomas Fire Sequences 1 (**a**), with active fire front delineations displayed in green, and 4 (**b**), with active fire front delineations starting as purple (earlier) and moving towards yellow (later).

4. Discussion

4.1. Dynamic Visualization of Wildfire Processes

4.1.1. Role of Visual/Descriptive Analysis of Wildfire Spread

The 3D geovisualization environment and fire features derived from rapid sequence ATIR imagery allowed users to examine relationships between topography, fuels, and instances of spotting in advance of the active fire front. Geovisualization tools developed through this study provide supplemental information to statistical analyses [42,45], particularly for visualizing patterns of active fronts and spread vectors, spread over multidirectional slope, and topographic and fuel controls on fire spread. While statistical analysis provides a more rigorous and less biased way of evaluating landscape-scale fuel and terrain controls on fire spread estimates, geovisualizations enable more nuanced explorations of fire behavior by visualizing relationships between fuels, weather, and topography. Statistical analyses also provide a quantitative characterization of the nature of the relationship between covariates, and descriptive analyses can supplement this analysis by providing more information regarding the relationships between covariates where the stratification scheme was ineffective, such as fire spread impedance at ridges or spread slowing along valley floors, which is addressed below [42].

In cases of fire spread over multidirectional slopes, elevation profiles displayed and analyzed alongside 3D geovisualizations of landscape-level wildfire behavior such as the ROSS provide additional information about topographic controls beyond the statistical analysis, such as detailed influence of fine-scale terrain features on fire spread and patterns of fire spread. The descriptive analysis of fire spread over multidirectional slopes expands on the findings that directional slope was the most explanatory covariate in the Schag et al. [42] study, accounting for over 50% of the variance of ROS estimates for three of the sequences.

The 10-m spatial resolution and enhanced topographic raster derived from the DEM were appropriate for the visual analysis of fine- and medium-scale topographic controls on fire spread. The spatial resolution of these products effectively facilitated the visualization of fine-scale topographic features, such as gullies or spurs, and medium-scale topographic features, such as ridges or valley floors. For the descriptive analyses, it is important to have a DEM or products derived from a DEM that can resolve landscape-scale topographic features; however, the utility of these products is limited by the uncertainty in the wildfire features derived from the ATIR imagery.

While the geovisualization environment enabled users to identify instances of spotting in advance of the active fire front, associations between spotting, fuels, and topography are inconclusive as the nearest hourly windspeeds did not indicate that higher windspeeds occurred during times of greater spotting activity, and no clear patterns between topography or fuels are visible. Finer temporal and spatial scale wind velocity and direction data are needed for a more conclusive understanding of spotting.

4.1.2. Evaluation of Custom Web-Based Geovisualization Environment

The web-based geovisualization tools were generally effective at facilitating the descriptive analyses of fire behavior. Users indicated the tools are useful for post-fire spread analysis and visualizing fire spread over multidirectional slopes, which aligns with the original intention of the tools. The ROSS was noted as being especially useful for analyzing relationships between spread vectors, slope, and weather through time. The ROS ellipse effectively portrays elliptical spread at each point along the fire front [13]. The visualizations generated through these ellipses are simpler but more limited in terms of visualizing patterns of ROS vector magnitude and terrain slope compared to the ROSS. The ROSS also displays upslope and downslope fire spread over time. It facilitates exploration of the relationships between spread vectors and the nearest hourly wind estimates from RAWS stations and the FireBuster model. By linking spread vectors in the ROSS and the map, users may visualize and explore relationships between fire spread, topography, fuels, and weather more effectively. User interface challenges such as difficulty selecting spread vectors in the ROSS and lack of interaction between the tools appeared to impact their utility and effectiveness and required the most overall improvement according to users. Users also remarked that the limited available data may have further hindered the utility of the geovisualization environment. The ease of navigation depended on previous experience with GIS as users who reported previous experience with GIS found the user interface easy to navigate, while those who did not found the tools to be unintuitive.

The latest iteration of the tools improved interactivity by highlighting selected spread vectors in the ROSS and the map, regardless of where it is selected (Figure 5). Improvements to interactivity in the user interface aimed to alleviate some of the challenges faced in earlier iterations.

Users suggested the most useful aspects of the geovisualization tools are visualizing fire spread over multidirectional slopes, inferring subtle qualitative relationships between fire spread, slope, and topography, and analyzing fire spread over time. However, the small sample size (n = 6) means that the findings from the survey should not be considered conclusive.

4.2. Descriptive Analysis of Wildfire Spread

4.2.1. Role of Topography

Both medium- and fine-scale topographic features appear to limit fire spread. Active fire perimeters often coincided with the crests of major ridgelines and contributed to the slowing of fire spread for Thomas Fire Sequences 1, 2, and 4. Ridgetops are likely associated with fire boundaries [39], with the clearest instances of these impedance features occurring for Thomas Fire Sequences 2 and 4. The change in directional slope of the fire spread coupled with the lower fire intensity associated with transitions in slope at major ridges likely contributed to fire spread impedance. Fire spread down the backside ridges typically decelerated or ceased in some cases for the Thomas Fire sequences. Fire spread deceleration along ridges was consistent across sequences regardless of the general directional trend of the sequence (i.e., fire spread parallel or perpendicular to major ridges), implying that ridges exert control over fire spread. Other studies have found that ridgetops may exhibit little control on fire extinguishment, yet the sparse fuels typically associated with ridges may result in the cessation of fire spread [41,44]. Conversely, Povak et al. [41] found that ridgetops provide minimal control on fire spread for all the ecoregions they analyzed, and valleys exert stronger control over fire spread. It is unclear if the adjacent areas to ridgelines burned prior to imaging, but visual analysis of the postfire NAIP imagery from July of 2018 shows the areas burned at some point. Had areas on opposite sides of the ridges burned during the Thomas Fire, it would be difficult to determine the extent to which the topography impedes fire spread and controls the location of the active perimeter compared to fuel controls.

Patterns of fire spread slowing along valley floors remained consistent between study areas, supporting other studies that found valleys to be associated with lower rates of spread or fire boundaries [39,41]. While spread along the valley floor was slower than spread on adjacent hillslopes for the sequences, some portions of Thomas Sequences 2 and 4 exhibited fast ROS rates along the valley floor. Despite fast ROS during the windier conditions of Thomas Fire Sequence 4, the presence of thicker riparian fuel types and higher variation in local topography, such as interlocking spurs and draws, underscore the contribution of topography and fuels to the slowing of fire spread. Similar control on fire spread was also observed during the last passes of Thomas Fire Sequence 2, as depicted in Figure 10.

Fire spread along minor topographic features such as spurs and draws appeared to be controlled topographically. Generally, fire spread tended to decelerate downslope on the backside of local spurs and accelerated upslope to the crest of spurs, often showing a local pattern of acceleration and deceleration at spurs and draws, respectively. Local transitions from upslope to downslope movement, along with denser fuel types and higher moisture levels in drainage areas, may contribute to deceleration of fire spread. At fine scales, fuel type and slope steepness were dominant influences on fire spread [39].

Steep (over 20 degrees) slopes in the direction of fire spread and homogeneous shrub fuels coincided with high ROS for all sequences with predominately upslope fire spread. These findings are consistent with past studies that analyze the relationships between fire spread, fire extent, and slope [18,19,40–42]. Areas of upslope fire spread through heterogeneous fuels and riparian areas also coincided with high ROS, implying topography may exert relatively more control over fire behavior than fuels for the study area. These findings corroborate those of Schag et al. [42], who found directional slope accounts for approximately 50% of the variance of ROS estimates for three of the sequences. However, ROS varied in topographically diverse areas, with cases of high ROS (e.g., Thomas Sequence 4) along with cases of low ROS (such as the north flank of Thomas Fire Sequence 2) occurring. Wind and fuel controls may have played a greater role in the control of fire spread in these instances, and at times likely contributed to the movement of the fire alongside local variation in terrain [44].

In sequences with predominantly downslope movement, such as Thomas Fire Sequence 3 and the Detwiler Fire, the fire generally spread slower than sequences with predominantly upslope movement, as expected. However, fine-scale topographic features such as draws and drainage gullies limit fire spread in a similar manner to sequences with predominantly upslope movement, such as impedance evident along the convergence of the NE front of Thomas Fire Sequence 1 and the SE front of Thomas Fire Sequence 3. These results imply that topography influences fire behavior at multiple spatial scales [39,42,43,45,46].

4.2.2. Role of Fuels

In addition to topography and weather, fuel composition and distribution play an integral role in influencing wildfire behavior. Homogeneous fuels consisting of either shrubs or herbaceous vegetation were mostly associated with areas of fast ROS, as exhibited by the fastest 95th percentile of magnitudes of ROS, nearly all of which spread upslope through homogeneous vegetation [42,43]. Schag et al. [30,42] found that the highest 95th percentile ROS estimates for spread vectors coincided with 90–100% shrub or herbaceous cover fractions, and the lowest 20% of ROS vectors were generally associated with more heterogeneous fuel types. The descriptive analyses support this finding. Fuel types in areas with the slowest ROS were typically composed of a mix of shrub and herbaceous vegetation with bare cover. Viedma et al. [43] and Holsinger et al. [39] found that fuel heterogeneity may be a control on fire spread. Areas of thick riparian vegetation along valley floors and in draws also coincided with the limits of fire perimeters and deceleration of fire spread, suggesting that these fuel types also exert control over fire spread by slowing the active front in these areas. The analyses also confirm that dense and mesic riparian vegetation limited fire spread to a greater extent than mixed shrub and herbaceous fuels in the study area. Patches of fuels and rock outcrops also slowed fire spread, even on steep terrain, as seen during Thomas Fire Sequence 1 (Figure 9). Holsinger et al. [39] stated that a combination of fuel types and topography may act as predominant controls on impeding fire spread in the southwestern region of the Unites States, which is consistent with the findings of this study. Some of the highest ROS rates for two of the Thomas fire sequences and the Detwiler fire sequence coincided with areas of heterogeneous fuel, implying that topography may contribute more control over fire spread than fuels overall for the study area. However, it is difficult to determine the relative contributions of weather during these sequences, and finer spatial and temporal scale wind data are needed to isolate the relative contributions of fuels, topography, and weather.

4.2.3. Other Factors Impeding Fire Spread

In addition to topographic and fuel-related controls on fire spread, roads impeded or stopped fire spread altogether. It is possible that coincidence between fire impedance, fire boundaries, and roads was due in part to the ability of roads to serve as defensible spaces in fire suppression efforts, especially for the sequences adjacent to SR33 near Thomas Fire Sequences 1–3 [44]. It is unclear to what extent fire suppression efforts played a role in limiting fire spread at roads; however, it is likely that fire suppression efforts along roads played a role in limiting fire spread in Thomas Fire Sequences 1–3. The ability of roads to impede fire spread depends on the directionality of fire spread in relation to the road. Fire spread perpendicular to SR33 typically crossed over the road, whereas fire spread parallel to the road coincided with the active boundary or impeded fire spread. Povak et al. [41] and Syphard et al. [38] found that fire boundaries or fuel breaks are often associated with roads. The fire behavior observed in this study is consistent with this type of behavior, supporting the findings of these previous studies.

5. Conclusions

5.1. Key Findings

The custom geovisualization tools were moderately effective for facilitating the descriptive analysis and visualization of fire spread over multidirectional slopes, differences in spread magnitudes within and between sequences over time, and inferring descriptive relationships between fire spread, fuels, slope, and topography. The ROSS effectively facilitated analysis of spread vectors, slope, and weather through time. The utility of the tools was primarily limited by user interface challenges, and the small sample size of the survey respondents (n = 6) indicated more testing is needed for these results to be conclusive.

The results of the analysis indicate medium- and fine-scale topographic features exerted control over fire spread. Minor topographic features such as spurs and draws controlled fire spread, with fuel type and slope steepness being dominant influences of fire spread at fine scales. Within the study area, fire spread consistently slowed or halted upon encountering major topographic features such as ridges or valleys. Roads and riparian fuels also coincided with cases of fire spread impedance, indicating they exerted control over fire behavior. Topography appeared to be a more dominant control over fire behavior than fuels for the study area [42] and appeared to influence fire behavior at multiple spatial scales [39,42,43,45,46]. It is difficult to determine the relative contribution of weather over fire behavior due to the lack of temporally and spatially fine-scale weather data. No conclusive relationships were found between spotting, fuels, and topography.

5.2. Challenges and Limitations

Weather, topography, and fuel play a key role in wildfire behavior. Isolating relationships between these factors at landscape scales is challenging, and there is little research related to statistically or descriptively analyzing landscape-scale covariates using rapid sequence repeat pass ATIR imagery [42]. Schag et al. [30,42] highlighted the challenges associated with the lack of finer spatial and temporal scale weather data. While hourly weather data from the nearest weather station or model estimates may indicate general wind direction and velocity for each sequence, their coarse temporal and spatial scales limit their effectiveness for isolating topographic and fuel-related controls on fire spread. The lack of this information at the requisite spatial and temporal scales makes it challenging to determine the relative contribution of weather on fire behavior in this study. Models such as the Coupled Atmosphere-Wildland-Fire-Environment (CAWFE) model [47–49] can provide detailed information about atmospheric and weather interactions during fire spread sequences, though such models are challenging to initiate, spin-up, and simulate particular sequences during extensive wildfire events. In addition to a lack of spatially and temporally fine-scale wind direction and velocity data, little information is available regarding areas that may have previously burned around the time of image acquisition for each sequence. Postfire NAIP imagery shows that the areas adjacent to the sequences burned at some point, but the timing is unclear.

In addition to these challenges, alternative methods for delineating spread vectors should be explored. The approach of Schag et al. [30,42] for delineating spread vectors consisted of generating evenly spaced points 30 m apart along the time = n (start) front curve, which were then used to generate local normal polyline connections to time $n + 1$. Using normalized spread vectors as landscape sampling units between sequences enabled the statistical analysis to be effectively carried out with minimal bias, but alternative methods may represent the actual fire spread more accurately [25]. An alternative method of generating spread vectors could incorporate a combination of the slope angle in the direction of spread and wind direction and velocity.

Obscurations in ATIR imagery due the smoke plume or pyrocumulus clouds generated by the fire pose challenges for accurately deriving fire fronts and other wildfire behavior features because some portions of the active fire may be obscured or distorted [50].

5.3. Future Research and Development

Further research pertaining to the utility of the geovisualization tools should be explored. One future research area regarding the utility of these tools mentioned by survey respondents and the Wildland Urban Interface Fire Operational Requirements and Capability Analysis Report of Findings is fire modeling accuracy and validation [5]. These tools could be developed to further support the visualization of simulation modeling results and validation efforts. Research pertaining to the general utility of 3D geovisualization tools in operational fire management and research contexts could also be explored. Future research could test the utility and effectiveness of these tools for visualizing other aspects of wildfire behavior or features not covered in this study, such as atmospheric and precipitation models or perimeter mapping.

Additional studies pertaining to descriptive analysis of wildfire behavior should explore fires in the same ecoregions as the Thomas and Detwiler fires and eventually be expanded to other ecoregions. Further research utilizing a combined statistical and descriptive approach for evaluating landscape-level wildfire behavior may be able to play on the strengths of both approaches when exploring the relationships between wildfire spread, topography, fuels, and weather.

Author Contributions: Conceptualization, K.S., D.A.S., A.N., P.R. and G.M.S.; methodology, K.S., D.A.S., A.N., P.R. and G.M.S.; formal analysis, K.S. and D.A.S.; resources, D.A.S., A.N., P.R. and G.M.S.; writing—original draft preparation, K.S., D.A.S., A.N. and P.R.; writing—review and editing D.A.S., A.N., P.R. and G.M.S.; funding acquisition D.A.S. and P.R. All authors have read and agreed to the published version of the manuscript.

Funding: Grant support from US Department of Agriculture Forest Service (Joint Venture Agreement G00012222) is acknowledged.

Institutional Review Board Statement: Not Applicable.

Informed Consent Statement: Not Applicable.

Data Availability Statement: The data that support the findings of this study are available upon request.

Acknowledgments: We used Esri ArcGIS Pro software to create figures for this study, and Esri ArcGIS Online to host the spatial data and the web map used in the geovisualization application.

Conflicts of Interest: The authors declare no conflict of interest.

Appendix A

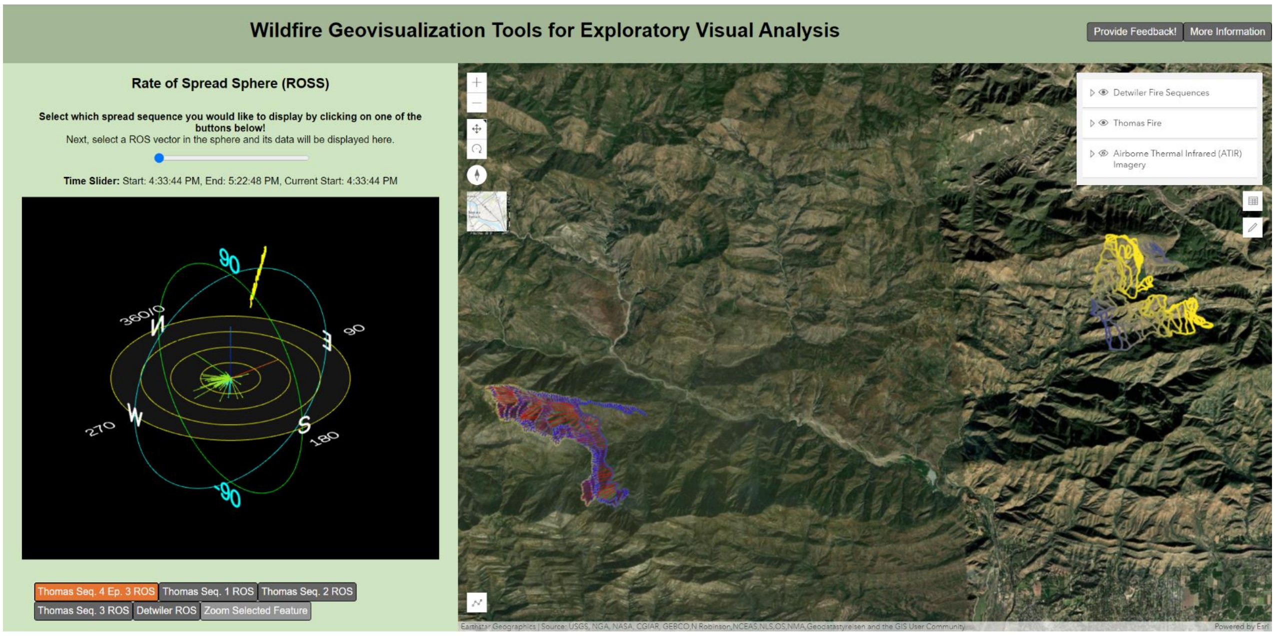

Figure A1. Web application layout.

Appendix B

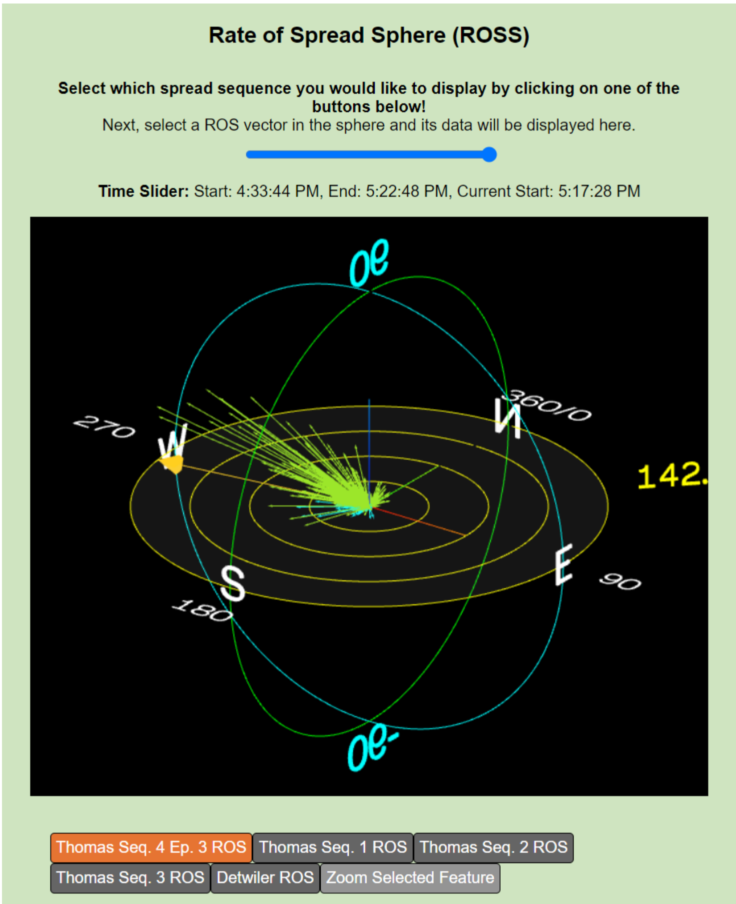

Figure A2. Rate of spread sphere.

Appendix C

Wildfire Geovisualization Tools Survey Questions

1. How would you describe the user interface and how can it be improved?
2. On a scale of 1 (easy) to 10 (difficult), how would you rate the user interface in terms of ease of use and navigation?
3. What aspects of rate of spread (ROS) do these visualization tools help you understand?
4. How does the Rate of Spread Sphere (ROSS) impact your understanding of the relationships between ROS vectors and these sequences of fire spread in general?
5. How would you rate the usefulness of the ROSS?
6. Were these tools useful for evaluating other aspects of landscape-level fire behavior, such as spread over multidirectional slope or fire spread impedance?
7. What aspects of the visualization tools were effective?
8. What aspects of the visualization tools were ineffective and how do you think they can be improved?
9. What additional features or tools would you like to see added?
10. Rate the effectiveness of the visualization tools for evaluating landscape-level wildfire behavior on a scale of 1 (ineffective) to 10 (effective).
11. What do you think these tools would be useful for?

References

1. Alexandre, P.M.; Mockrin, M.H.; Stewart, S.I.; Hammer, R.B.; Radeloff, V.C. Rebuilding and new housing development after wildfire. *Int. J. Wildland Fire* **2014**, *24*, 138–149. [CrossRef]
2. Radeloff, V.C.; Helmers, D.P.; Anu Kramer, H.; Mockrin, M.H.; Alexandre, P.M.; Bar-Massada, A.; Bustic, V.; Hawbaker, T.J.; Martinuzzi, S.; Syphard, A.D.; et al. Rapid growth of the US wildland-urban interface raises wildfire risk. *Proc. Natl. Acad. Sci. USA* **2018**, *115*, 3314–3319. [CrossRef]
3. Dennison, P.E.; Brewer, S.C.; Arnold, J.D.; Moritz, M.A. Large wildfire trends in the western United States, 1984–2011. *Geophys. Res. Lett.* **2014**, *41*, 2928–2933. [CrossRef]
4. Halsey, R.W. *Fire, Chaparral, and Survival in Southern California*, 2nd ed.; Marino, K., Ed.; Sunbelt Publications, Inc.: San Diego, CA, USA, 2008; ISBN 978-093-265-369-7.
5. Berlin, G.; Hieb, M. *Wildland Urban Interface Fire Operational Requirements and Capability Analysis—Report of Findings*; U.S. Department of Homeland Security: Washington, DC, USA; U.S. Fire Administration: Emmitsburg, MD, USA; Federal Emergency Management Agency: Washington, DC, USA, 2019.
6. Finney, M.A. *FARSITE: Fire Area Simulator—Model Development and Evaluation*; RMRS-RP-4; USDA Forest Service, Rocky Mountain Research Station: Fort Collins, CO, USA, 1998; pp. 1–36.
7. Ramírez, J.; Monedero, S.; Buckley, D. New approaches in fire simulations analysis with Wildfire Analyst. In Proceedings of the 5th International Wildland Fire Conference, Sun City, South Africa, 9–13 May 2011. [CrossRef]
8. Bogdos, N.; Manolakos, E.S. A tool for simulation and geo-animation of wildfires with fuel editing and hotspot monitoring capabilities. *Environ. Model. Softw.* **2013**, *46*, 182–195. [CrossRef]
9. Crawl, D.; Block, J.; Lin, K.; Altintas, I. Firemap: A Dynamic Data-Driven Predictive Wildfire Modeling and Visualization Environment. *Procedia Comput. Sci.* **2017**, *108C*, 2230–2239. [CrossRef]
10. You, J.; Huai, Y.; Nie, X.; Chen, Y. Real-time 3D visualization of forest fire spread based on tree morphology and finite state machine. *Comput. Graph.* **2022**, *103*, 109–120. [CrossRef]
11. Çöltekin, A.; Bleisch, S.; Andrienko, G.; Dykes, J. Persistent challenges in geovisualization—A community perspective. *Int. J. Cartogr.* **2017**, *3*, 115–139. [CrossRef]
12. Rothermel, R.C. *How to Predict the Spread and Intensity of Forest and Range Fires*; INT-143; United States Department of Agriculture Forest Service: Ogden, UT, USA, 1983.
13. Anderson, D.H.; Catchpole, E.A.; De Mestre, N.J.; Parkes, T. Modelling the spread of grass fires. *J. Aust. Math. Soc. Ser. B. Appl. Math.* **1982**, *23*, 451–466. [CrossRef]
14. Sullivan, A.L. Wildland surface fire spread modelling, 1990–2007. 3: Simulation and mathematical analogue models. *Int. J. Wildland Fire* **2009**, *18*, 387–403. [CrossRef]
15. Opach, T.; Rød, J.K. Cartographic visualization of vulnerability to natural hazards. *Cartographica* **2013**, *48*, 113–125. [CrossRef]
16. Stow, D.A.; Riggan, P.J.; Storey, E.J.; Coulter, L.L. Measuring fire spread rates from repeat pass airborne thermal infrared imagery. *Remote Sens. Lett.* **2014**, *5*, 803–812. [CrossRef]
17. Stow, D.; Riggan, P.; Schag, G.; Brewer, W.; Tissell, R.; Coen, J.; Storey, E. Assessing uncertainty and demonstrating potential for estimating fire rate of spread at landscape scales based on time sequential airborne thermal infrared imaging. *Int. J. Remote Sens.* **2019**, *40*, 4876–4897. [CrossRef]

18. Butler, B.W.; Anderson, W.R.; Catchpole, E.A. Influence of Slope on Fire Spread Rate. In Proceedings of the Fire Environment—Innovations, Management, and Policy, Destin, FL, USA, 26–30 March 2007; pp. 75–82.
19. Viegas, D.X. Slope and wind effects on fire propagation. *Int. J. Wildland Fire* **2004**, *13*, 143–156. [CrossRef]
20. Salvoldi, M.; Siaki, G.; Sprintsin, M.; Karnieli, A. Burned Area Mapping Using Multi-Temporal Sentinel-2 Data by Applying the Relative Differenced Aerosol-Free Vegetation Index (RdAFRI). *Remote Sens.* **2020**, *12*, 2753. [CrossRef]
21. Farhadi, H.; Ebadi, H.; Kiani, A. Badi: A Novel Burned Area Detection Index for Sentinel-2 Imagery Using Google Earth Engine Platform. *ISPRS Ann. Photogramm. Remote Sens. Spat. Inf. Sci.* **2023**, *10*, 179–186. [CrossRef]
22. Riggan, P.J.; Tissell, R.G. Chapter 6: Airborne remote sensing of wildland fires. *Dev. Environ. Sci.* **2009**, *8*, 139–168. [CrossRef]
23. Hoffman, J.W.; Coulter, L.L.; Luciani, E.M.; Riggan, P.J. Rapid turn-around mapping of wildfires and disasters with airborne infrared imagery from the new Firemapper® 2.0 and Oilmapper systems. In Proceedings of the American Society for Photogrammetry and Remote Sensing Annual Conference, Baltimore, MD, USA, 7–11 March 2005; pp. 363–370.
24. Riggan, P.J.; Hoffman, J.W. FireMapper: A thermal-imaging radiometer for wildfire research and operations. In Proceedings of the IEEE Aerospace Conference, Big Sky, MT, USA, 8–15 March 2003.
25. Moran, C.J.; Seielstad, C.A.; Cunningham, M.R.; Hoff, V.; Parsons, R.A.; Queen, L.; Sauerbrey, K.; Wallace, T. Deriving Fire Behavior Metrics from UAS Imagery. *Fire* **2019**, *2*, 36. [CrossRef]
26. Esri. "World Topographic Map" [Tile Layer]. Scale Not Given. "World Topographic Map". 26 October 2017. Available online: https://www.arcgis.com/home/item.html?id=7dc6cea0b1764a1f9af2e679f642f0f5 (accessed on 8 January 2021).
27. Langridge, R. *Central Coast Region Report*; SUM-CCCA4-2018-006; California's Fourth Climate Change Assessment: Santa Cruz, CA, USA, 2018.
28. Kolden, C.; Abatzoglou, J. Spatial Distribution of Wildfires Ignited under Katabatic vs. Non-Katabatic Winds in Mediterranean Southern California USA. *Fire* **2018**, *1*, 19. [CrossRef]
29. Esri. "World Hillshade" [Tile Layer]. Scale Not Given. "World Hillshade". 9 July 2015. Available online: https://www.arcgis.com/home/item.html?id=1b243539f4514b6ba35e7d995890db1d (accessed on 8 January 2021).
30. Schag, G.M.; Stow, D.A.; Riggan, P.J.; Tissell, R.G.; Coen, J.L. Examining Landscape-Scale Fuel and Terrain Controls of Wildfire Spread Rates Using Repetitive Airborne Thermal Infrared (ATIR) Imagery. *Fire* **2021**, *4*, 6. [CrossRef]
31. National Elevation Dataset (NED), United States Geological Survey (USGS). Available online: https://www.usgs.gov/3d-elevation-program (accessed on 1 August 2020).
32. National Agriculture Imagery Program (NAIP), United States Geological Survey (USGS). Available online: https://www.usgs.gov/centers/eros/science/usgs-eros-archive-aerial-photography-national-agriculture-imagery-program-naip?qt-science_center_objects=0#qt-science_center_objects (accessed on 1 March 2020).
33. Gorelick, N.; Hancher, M.; Dixon, M.; Ilyushchenko, S.; Thau, D.; Moore, R. Google Earth Engine: Planetary-scale geospatial analysis for everyone. *Remote Sens. Environ.* **2017**, *202*, 18–27. [CrossRef]
34. Three.js Contributors; *Three.js JavaScript 3D Library*, version r125. 2021. Available online: https://threejs.org/ (accessed on 5 February 2021).
35. Esri. *ArcGIS API for JavaScript*, version 4.18; Esri Inc.: Redlands, CA, USA, 2020.
36. Benoit, J.W.; Chen, S.-C. FireBuster: A tool for fire management. In *Proceedings of the Fifth International Symposium on Fire Economics, Planning, and Policy: Ecosystem Services and Wildfires*; General Technical Report PSW-GTR-261 (English); González-Cabán, A., Sánchez, J.J., Eds.; Department of Agriculture, Forest Service, Pacific Southwest Research Station: Albany, CA, USA, 2019; pp. 25–37.
37. Esri. *ArcGIS Survey123*; Esri Inc.: Redlands, CA, USA, 2020.
38. Syphard, A.D.; Keeley, J.E.; Brennan, T.J. Comparing the role of fuel breaks across southern California national forests. *Forest. Ecol. Manag.* **2011**, *261*, 2038–2048. [CrossRef]
39. Holsinger, L.; Parks, S.A.; Miller, C. Weather, fuels, and topography impede wildland fire spread in western US landscapes. *Forest. Ecol. Manag.* **2016**, *380*, 59–69. [CrossRef]
40. Mermoz, M.; Kitzberger, T.; Veblen, T. Landscape influences on occurrence and spread of wildfires in Patagonian forests and shrublands. *Ecology* **2005**, *86*, 2705–2715. [CrossRef]
41. Povak, N.A.; Hessburg, P.F.; Salter, R.B. Evidence for scale-dependent topographic controls on wildfire spread. *Ecosphere* **2018**, *9*, e02443. [CrossRef]
42. Schag, G.; Stow, D.; Riggan, P.; Nara, A. Spatial-statistical analysis of landscape-level wildfire rate of spread. *Remote Sens.* **2022**, *14*, 3980. [CrossRef]
43. Viedma, O.; Angeler, D.G.; Moreno, J.M. Landscape structural features control fire size in a Mediterranean forested area of central Spain. *Int. J. Wildland Fire* **2009**, *18*, 575–583. [CrossRef]
44. Narayanaraj, G.; Wimberly, M.C. Influences of forest roads on the spatial pattern of wildfire boundaries. *Int. J. Wildland Fire* **2011**, *20*, 792–803. [CrossRef]
45. Viedma, O.; Quesada, J.; Torres, I.; De Santis, A.; Moreno, J.M. Fire severity in a large fire in a Pinus pinaster forest is highly predictable from burning conditions, stand structure, and topography. *Ecosystems* **2015**, *18*, 237–250. [CrossRef]
46. Sharples, J.J.; McRae, R.H.; Wilkes, S.R. Wind–terrain effects on the propagation of wildfires in rugged terrain: Fire channeling. *Int. J. Wildland Fire* **2012**, *21*, 282–296. [CrossRef]

47. Coen, J.L.; Riggan, P.J. Simulation and thermal imaging of the 2006 Esperanza Wildfire in southern California: Application of a coupled weather-wildland fire model. *Int. J. Wildland Fire* **2014**, *23*, 755–770. [CrossRef]
48. Coen, J.L. Simulation of the Big Elk Fire using coupled atmosphere–fire modeling. *Int. J. Wildland Fire* **2005**, *14*, 49–59. [CrossRef]
49. Clark, T.L.; Jenkins, M.A.; Coen, J.; Packham, D. A coupled atmosphere–fire model: Role of the convective Froude number and dynamic fingering at the fireline. *Int. J. Wildland Fire* **1996**, *6*, 177–190. [CrossRef]
50. Riggan, P.J.; Tissell, R.G.; Lockwood, R.N. Remote measurement of the 1992 Tapera prescribed fire at the Reserva Ecologica do IBGE. In *Efeitos do Regime do Fogo Sobre a Estrutura de Comunidades de Cerrado: Resultados do Projeto Fogo*; Miranda, H.S., Ed.; IBAMA: Brasilia, Brazil, 2010; pp. 35–46, ISBN 978-85-7300-305-5.

Disclaimer/Publisher's Note: The statements, opinions and data contained in all publications are solely those of the individual author(s) and contributor(s) and not of MDPI and/or the editor(s). MDPI and/or the editor(s) disclaim responsibility for any injury to people or property resulting from any ideas, methods, instructions or products referred to in the content.